ELSEVIER

International Journal of Solids and Structures 41 (2004) 5087–5104

INTERNATIONAL JOURNAL OF SOLIDS and STRUCTURES

www.elsevier.com/locate/ijsolstr

Modeling nonlinear peeling of ductile thin films—critical assessment of analytical bending models using FE simulations

Yueguang Wei *

State–Key Laboratory of Nonlinear Mechanics (LNM), Institute of Mechanics, Chinese Academy of Sciences, Beijing 100080, PR China

Received 4 December 2003; received in revised form 2 April 2004
Available online 18 May 2004

Abstract

Three analytical double-parameter criteria based on a bending model and a two-dimensional finite element analysis model are presented for the modeling of ductile thin film undergoing a nonlinear peeling process. The bending model is based on different governing parameters: (1) the interfacial fracture toughness and the separation strength, (2) the interfacial fracture toughness and the crack tip slope angle, and (3) the interfacial fracture toughness and the critical Mises effective strain of the delaminated thin film at the crack tip. Thin film nonlinear peeling under steady-state condition is solved with the different governing parameters. In addition, the peeling test problem is simulated by using the elastic–plastic finite element analysis model. A critical assessment of the three analytical bending models is made by comparison of the bending model solutions with the finite element analysis model solutions. Furthermore, through analyses and comparisons for solutions based on both the bending model and the finite element analysis model, some connections between the bending model and the finite element analysis model are developed. Moreover, in the present research, the effect of different selections for cohesive zone shape on the ductile film peeling solutions is discussed.

Keywords: Peel test; Nonlinear peeling; Thin film; Double-parameter criterion; Bending model; Fracture toughness

1. Introduction

The fundamental roles of thin films in modern materials are not only in protection and connection, but also in strengthening or toughening. In addition, thin films also play an important role in extending the multi-functions of modern materials. In order to check the adhesion property and separation strength between a thin film and a substrate, a simple test method, called peel test, was designed 50 years ago by Spies (1953). Due to simplicity of the test method to be operated, the peel test has been widely applied in many research areas (Feliu-Baez et al., 2001; Choi and Oh, 2001; Asai et al., 2001; Bundy et al., 2000;

* Tel.: +86-10-62648721; fax: +86-10-62561284.
E-mail address: ywei@lnm.imech.ac.cn (Y. Wei).

0020-7683/$ - see front matter © 2004 Elsevier Ltd. All rights reserved.
doi:10.1016/j.ijsolstr.2004.04.026

Kawabe et al., 2000). Specifically, when both the thin film and the substrate can be considered as elastic materials, the interfacial adhesion properties (adhesion toughness) can be obtained directly by measuring the peel force. Actually, the peel force per unit length (i.e., energy release rate of system) is equal to the interfacial adhesion energy per unit area (toughness) from considering energy balance of total system. However, when the thin film is a ductile material, the measured peel force is often much larger than the interfacial toughness. Plastic dissipation due to plastic loading and unloading occurs during the peeling process. The plastic dissipation increases the exerted peel force in order to allow the thin film delamination. In order to model the increase of the energy release rate (or peeling force) due to plastic dissipation, Kim and his coworkers (Kim and Aravas, 1988; Kim and Kim, 1988; Kim et al., 1989) presented a plastic bending model to predict the plastic dissipation of ductile thin films. In the decade following that with most analyses on ductile thin film peeling adopted or referred to this bending model (Kinloch et al., 1994; Moidu et al., 1998; Park and Yu, 1998; Yang et al., 1999). Wei and Hutchinson (1998) adopted a different method to analyze elastic–plastic film peeling process. In their analysis, the thin film steady-state delaminating process was simulated by using the elastic–plastic finite element method under 2D plane strain conditions, except for the detached part of thin film which was still described by the bending model. They obtained qualitatively and quantitatively different result from that based on the bending model. An important question is thus: what model is the most reliable? Considering that the bending model is simple and easily can be used to interpret applications, one wants to know the condition under which the bending model result is reliable.

Considering that the peel test is widely applied and plays an important role in thin film engineering, it is very important and necessary to clear up that point. For this purpose, several experts (Cotterell et al., 2002) recently proposed a round robin on the analysis of the peel test involving a comparison research on Kim model and Wei–Hutchinson model.

Usually, a complete characterization on an elastic–plastic crack growth process requires a double-parameter criterion (Rice, 1974; Betegon and Hancock, 1991; O'Dowd and Shih, 1991; Wei and Wang, 1995). Since the peeling process of the ductile thin film is an elastic–plastic interfacial separation (fracture) process, double-parameter criterion is thus needed to characterize the process. In the present research, three double-parameter criteria will be adopted in order to describe the peeling process for the ductile thin film, based on both the bending model and the two-dimensional elastic–plastic finite element analysis model. The detailed solutions are solved for each double-parameter criterion. The characterization of both the interfacial adhesion toughness and the crack tip slope angle adopted by Kim and his collaborators (see Kim and Aravas, 1988; Kim and Kim, 1988; Kim et al., 1989) is only one of the three criteria in the present research. By analysis and comparing the bending model results with those based on the finite element analysis model from Wei and Hutchinson (1998), the connection between two model solutions is presented. Furthermore, the reliabilities of the bending models will be discussed.

2. Bending model and delaminating criteria in peel test

The deformation process of elastic–plastic thin film in a peeling test is described in Fig. 1. Thin film is subjected to an external force P and undergoes delamination, plastic loading and unloading segments OA, AB and BD in the graph of Fig. 1 are referred to the elastic bending, elastic–plastic bending as well as the unloading bending, respectively. DE is referred to the reverse plastic bending. State E shows that the portion of thin film is pulled into straight line and the corresponding film curvature within the portion is zero. The section EF is the second unloading state. The detailed relation between moment and curvature will be derived in the following section.

The ductile thin film peeling process and delamination along the substrate can be characterized by the double-parameter criterion (an elastic delamination is usually characterized by a single-parameter crite-

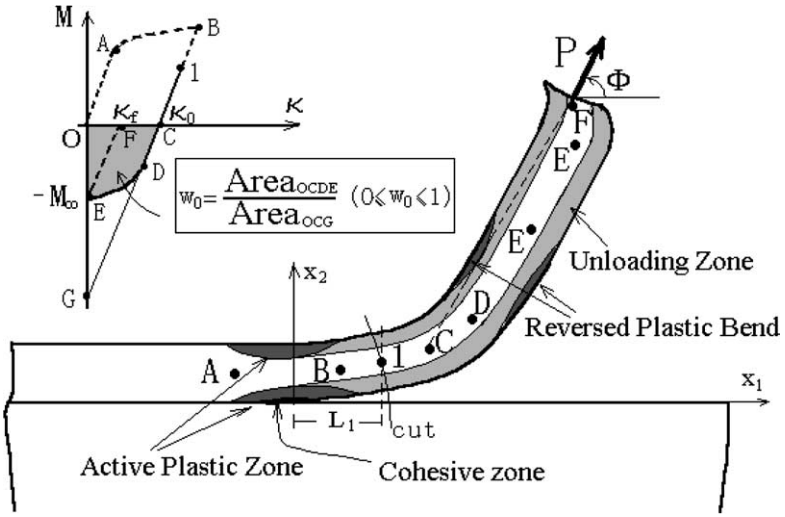

Fig. 1. Bend deformation and simplified model for thin film nonlinear peeling process.

rion). Two independent parameters are needed to characterize two main factors, interfacial adhesion property and the plastic dissipation. In the present research, three double-parameter criteria will be used to describe the elastic–plastic peeling process for thin film, which are described in Fig. 2(b)–(d), respectively. Fig. 2(b) corresponds to the conventional cohesive model, the independent parameters of this model are $(\Gamma_0, \hat{\sigma})$, where Γ_0 is interfacial fracture toughness, or adhesion energy per unit area, $\hat{\sigma}$ is the interfacial separation strength. Fig. 2(c) corresponds to a model based on taking the interfacial adhesion toughness Γ_0 and the crack tip critical slope angle θ^c_{tip} as the governing parameters for describing the peeling process. This characterization was first adopted by Kim and his coworkers (see Kim and Aravas, 1988; Kim and Kim, 1988; Kim et al., 1989). Fig. 2(d) corresponds to a model based on two parameters $(\Gamma_0, \bar{\varepsilon}_c)$, where $\bar{\varepsilon}_c$ is the critical value of Mises effective strain at the crack tip for thin film. This model is a new model described in

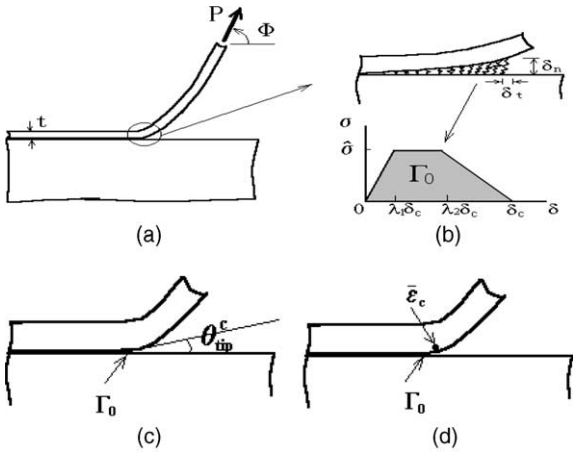

Fig. 2. Bending model and three double-parameter criteria for peeling test. (a) Peel test, (b) $(\Gamma_0, \hat{\sigma})$ criterion, (c) $(\Gamma_0, \theta^c_{tip})$ criterion, (d) $(\Gamma_0, \bar{\varepsilon}_c)$ criterion, $\bar{\varepsilon}_c$ is Mises effective strain.

the present paper. Combining these two independent parameters and the relationship of the elastic–plastic bending, one can derive the solutions for the elastic–plastic peeling process.

It is very important to set up a relationship between the peeling force P (total energy release rate of the system), and the interfacial adhesion toughness Γ_0, as well as the geometrical and physical parameters of the thin film and substrate in the peel test research. Under steady-state condition, the energy balance requires:

$$P(1-\cos\Phi)=\Gamma_0 \tag{1}$$

for elastic peeling process, and

$$P(1-\cos\Phi)=\Gamma_0+\Gamma^{\mathrm{p}} \tag{2}$$

for elastic–plastic peeling process. Where Γ^{p} is the plastic dissipation or the increase of energy release rate caused by the plastic dissipation. In the following sections, based on the stress–strain analysis for thin film, the fundamental relations for thin film nonlinear peeling process and a relationship for Γ^{p} will be derived.

3. Fundamental relations for bending model

Kim and Aravas (1988) derived the fundamental relations for thin film elastic–plastic peeling process based on a beam bending model in the case of incompressible material conditions ($v=1/2$). In the present section, the fundamental bending relations will be derived for the general case of the compressible materials.

Suppose that the uni-directional stress–strain relation for thin film material can be characterized using a power-law hardening relation:

$$\sigma=\begin{cases} E\varepsilon, & \text{if } \sigma\leqslant\sigma_{\mathrm{Y}},\\ \sigma_{\mathrm{Y}}(\varepsilon/\varepsilon_{\mathrm{Y}})^{N}, & \text{if } \sigma\geqslant\sigma_{\mathrm{Y}}, \end{cases} \tag{3}$$

where $(E,\sigma_{\mathrm{Y}},N)$ are the Young's modulus, yield strength and strain hardening exponent, respectively, and $\varepsilon_{\mathrm{Y}}=\sigma_{\mathrm{Y}}/E$ is the yield strain. Eq. (3) can be generalized to a multi-axis stress case as

$$\bar{\sigma}=\begin{cases} \left(\frac{3}{2}E/(1+v)\right)\bar{\varepsilon}, & \text{if } \bar{\sigma}\leqslant\sigma_{\mathrm{Y}},\\ \sigma_{\mathrm{Y}}(\bar{\varepsilon}/\bar{\varepsilon}_{\mathrm{Y}})^{N}, & \text{if } \bar{\sigma}\geqslant\sigma_{\mathrm{Y}}, \end{cases} \tag{4}$$

where v is Poisson's ratio, while $\bar{\sigma}$ and $\bar{\varepsilon}$ are the effective stress and effective strain defined by

$$\bar{\sigma}=\left(\frac{3}{2}\sigma'_{ij}\sigma'_{ij}\right)^{1/2},\quad \bar{\varepsilon}=\left(\frac{2}{3}\varepsilon'_{ij}\varepsilon'_{ij}\right)^{1/2} \tag{5}$$

in which $\sigma'_{ij}=\sigma_{ij}-\frac{1}{3}\sigma_{kk}\delta_{ij}$ and $\varepsilon'_{ij}=\varepsilon_{ij}-\frac{1}{3}\varepsilon_{kk}\delta_{ij}$ are the deviatoric stress and deviatoric strain, and

$$\bar{\varepsilon}_{\mathrm{Y}}=\sigma_{\mathrm{Y}}\Big/\left[\frac{3}{2}E/(1+v)\right]=\varepsilon_{\mathrm{Y}}\Big/\left[\frac{3}{2}/(1+v)\right]. \tag{6}$$

As usual, let us suppose that the thin film can undertake normal stress only, and that shear stress can be neglected. According to this assumption, besides $\sigma_{ij}=0$, $\varepsilon_{ij}=0$ $(i\neq j)$, the stress and strain states within the thin film under plane strain condition are given by (see Fig. 3 for coordinate system):

$$\sigma_{11}=\sigma,\quad \sigma_{22}\neq 0,\quad \sigma_{33}=0,\quad \varepsilon_{11}=\varepsilon,\quad \varepsilon_{22}=0,\quad \varepsilon_{33}\neq 0, \tag{7}$$

where σ and ε are the stress and strain components along the x-direction on the x-coordinate plane. Stress and strain components satisfy the following constitutive relations:

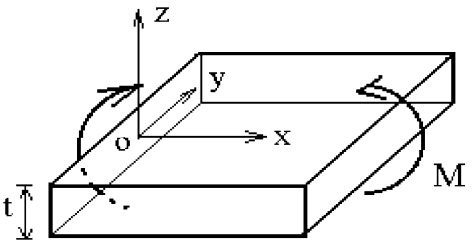

Fig. 3. Bend model description.

$$\varepsilon_{ij} = \frac{1}{E}[(1+v)\sigma_{ij} - v\sigma_{kk}\delta_{ij}] \tag{8}$$

for elastic loading, and

$$\begin{aligned} &\varepsilon_{ij}^{e} = \frac{1}{E}[(1+v)\sigma_{ij} - v\sigma_{kk}\delta_{ij}], \quad \varepsilon_{ij}^{p} = \lambda\sigma'_{ij} = \frac{3\varepsilon^{p}}{2\bar{\sigma}}\sigma'_{ij}, \\ &\varepsilon_{ij} = \varepsilon_{ij}^{e} + \varepsilon_{ij}^{p} = \left(\frac{1+v}{E} + \lambda\right)\sigma_{ij} - \left(\frac{v}{E} + \frac{\lambda}{3}\right)\sigma_{kk}\delta_{ij} \end{aligned} \tag{9}$$

for elastic–plastic loading. For power-law hardening materials (see Eq. (4)), λ in Eq. (9) is obtained as

$$\lambda = \frac{3\varepsilon^{p}}{2\bar{\sigma}} = \frac{(1+v)}{E}\left[\left(\frac{\bar{\sigma}}{\sigma_{Y}}\right)^{1/N-1} - 1\right]. \tag{10}$$

Using the plane strain condition $\varepsilon_{22} = 0$, one derives out

$$\begin{aligned} &\sigma_{11} = \sigma, \quad \sigma_{22} = v\sigma, \quad \sigma_{33} = 0, \\ &\varepsilon_{11} = (1-v^2)\sigma/E = \varepsilon, \quad \varepsilon_{22} = 0, \quad \varepsilon_{33} = -v(1+v)\sigma/E = -[v/(1-v)]\varepsilon \end{aligned} \tag{11}$$

for elastic loading, and

$$\begin{aligned} &\sigma_{11} = \sigma, \quad \sigma_{22} = \alpha\sigma, \quad \sigma_{33} = 0, \\ &\varepsilon_{11} = \varepsilon, \quad \varepsilon_{22} = 0, \quad \varepsilon_{33} = -[\alpha/(1-\alpha)]\varepsilon \end{aligned} \tag{12}$$

for elastic–plastic loading, where

$$\alpha = \frac{1}{2}[1 - U_0(\bar{\sigma}/\sigma_{Y})], \quad U_0(\bar{\sigma}/\sigma_{Y}) = \frac{(1-2v)}{1 + \frac{2}{3}(1+v)[(\bar{\sigma}/\sigma_{Y})^{1/N-1} - 1]}. \tag{13}$$

Thus, effective stress and effective strain expressed by stress and strain components in x-coordinate for elastic case and elastic–plastic case can be found:

$$\bar{\sigma} = \sqrt{1 - v + v^2}|\sigma|, \quad \bar{\varepsilon} = \frac{2\sqrt{1 - v + v^2}}{3(1-v)}|\varepsilon| \tag{14}$$

for elastic loading, and

$$\bar{\sigma} = \sqrt{1 - \alpha + \alpha^2}|\sigma|, \quad \bar{\varepsilon} = \frac{2\sqrt{1 - \alpha + \alpha^2}}{3(1-\alpha)}|\varepsilon| \tag{15}$$

for elastic–plastic loading.

Strain component in x-direction for thin film bending can be expressed as

$$\varepsilon = -\kappa z, \tag{16}$$

where $\kappa = \mathrm{d}\theta/\mathrm{d}s$ is the curvature of the medium plane ($z = 0$), θ is the slope angle of the medium plane with respect to the x-coordinate. The bending moment can be calculated from integral formula

$$M = 2\int_0^{t/2} |\sigma| z \,\mathrm{d}z. \tag{17}$$

3.1. Elastic bending

During elastic bending, from Eqs. (11), (16) and (17) one can derive the relationship between the bending moment and the curvature as

$$\frac{M}{M_0} = \frac{2\kappa}{3\kappa_\mathrm{e}}, \tag{18}$$

where $M_0 = \frac{3}{2}M_\mathrm{e}$ is the limit bending moment for perfectly plastic material, where M_e and κ_e are the elastic limit moment and elastic limit curvature, respectively. The expressions for M_e and κ_e are

$$M_\mathrm{e} = \frac{2}{3}M_0 = \frac{\sigma_\mathrm{Y} t^2}{6\sqrt{1-v+v^2}}, \quad \kappa_\mathrm{e} = \frac{2(1-v^2)\sigma_\mathrm{Y}}{Et\sqrt{1-v+v^2}}. \tag{19}$$

3.2. Elastic–plastic bending

From the power-law hardening relationship $\bar{\sigma} = \sigma_\mathrm{Y}(\bar{\varepsilon}/\bar{\varepsilon}_\mathrm{Y})^N$ (see (4)) and the expressions for the effective stress and effective strain (see Eq. (15)), one obtains

$$|\sigma| = \sigma_\mathrm{Y}^\mathrm{e}\frac{\sqrt{1-v+v^2}}{\sqrt{1-\alpha+\alpha^2}}\left[\frac{(1-v)}{\sqrt{1-v+v^2}}\frac{\sqrt{1-\alpha+\alpha^2}}{(1-\alpha)}\frac{|\varepsilon|}{\varepsilon_\mathrm{Y}^\mathrm{e}}\right]^N, \tag{20}$$

where

$$\sigma_\mathrm{Y}^\mathrm{e} = \frac{\sigma_\mathrm{Y}}{\sqrt{1-v+v^2}}, \quad \varepsilon_\mathrm{Y}^\mathrm{e} = \frac{(1-v^2)\sigma_\mathrm{Y}}{E\sqrt{1-v+v^2}} \tag{21}$$

are the maximum stress and strain in the x-direction in the case of elastic limit bending. From Eqs. (11), (16), (17) and (20), the bending moment can be written as

$$\begin{aligned} M &= 2\int_0^{t/2} |\sigma| z \,\mathrm{d}z = 2\int_0^{\xi} |\sigma| z \,\mathrm{d}z + 2\int_\xi^{t/2} |\sigma| z \,\mathrm{d}z \\ &= \frac{2E\kappa\xi^3}{3(1-v^2)} + 2\sigma_\mathrm{Y}^\mathrm{e}\sqrt{1-v+v^2}\left[\frac{(1-v)}{\sqrt{1-v+v^2}}\frac{\kappa}{\kappa_\mathrm{e} t/2}\right]^N \int_\xi^{t/2} \frac{1}{\sqrt{1-\alpha+\alpha^2}}\left[\frac{\sqrt{1-\alpha+\alpha^2}}{(1-\alpha)}\right]^N z^{N+1}\,\mathrm{d}z, \end{aligned} \tag{22a}$$

where $z = \xi$ is the distance between the intersection of the elastic zone and the plastic zone with the medium layer for a rectangle section. The moment–curvature relationship can be evaluated numerically by using Eqs. (4), (13), (15) and (16). An approximately analytical solution can be derived. Firstly, it is interesting to analyze the values of the function $U_0(\bar{\sigma}/\sigma_\mathrm{Y})$ from Eq. (13), as shown in Table 1. Obviously, the value of

Table 1
The variation of function $U_0(\bar{\sigma}/\sigma_Y)$ with material parameters v and N

		$\bar{\sigma}/\sigma_Y$			
		1.2	1.5	2.0	2.5
$N = 0.1$	$v = 0.5$	0.000	0.0000	0.0000	0.0000
	$v = 0.4$	0.041	0.0056	0.0004	0.0001
	$v = 0.3$	0.087	0.0120	0.0009	0.0001
	$v = 0.2$	0.138	0.0190	0.0015	0.0002
$N = 0.2$	$v = 0.5$	0.000	0.0000	0.0000	0.0000
	$v = 0.4$	0.099	0.0420	0.0133	0.0055
	$v = 0.3$	0.207	0.0880	0.0280	0.0120
	$v = 0.2$	0.322	0.1411	0.0461	0.0191

function U_0 is much smaller than 1 within the effective region of the normalized effective stress $\bar{\sigma}/\sigma_Y$. Thus, α in the integral of Eq. (22a) can be expanded in terms of U_0,

$$M = \frac{2E\kappa\xi^3}{3(1-v^2)} + 2\sigma_Y^e\sqrt{1-v+v^2}\left[\frac{(1-v)}{\sqrt{1-v+v^2}}\frac{\kappa}{\kappa_e t/2}\right]^N \frac{2}{\sqrt{3}^{1-N}} \times \int_{\xi}^{t/2}\left\{1 - NU_0 + \left(\frac{1}{2}N^2 + \frac{2}{3}N - \frac{1}{6}\right)U_0^2 + \cdots\right\} z^{N+1}\,\mathrm{d}z. \tag{22}$$

The coefficients in the series expansion of the last formula are small quantities, and the influence from each terms can be neglected, leading to

$$M = \frac{2E\kappa\xi^3}{3(1-v^2)} + 2\sigma_Y^e\sqrt{1-v+v^2}\left[\frac{(1-v)}{\sqrt{1-v+v^2}}\frac{\kappa}{\kappa_e t/2}\right]^N \frac{2}{\sqrt{3}^{1-N}(N+2)}\left\{\left(\frac{t}{2}\right)^{N+2} - \xi^{N+2}\right\}. \tag{23}$$

On the other hand, from Eq. (13) U_0 decreases monotonically with increasing $\bar{\sigma}/\sigma_Y$, and its maximum and minimum are equal to 1–2v and 0, respectively. Eq. (23) corresponds to $U_0 = 0$. Let U_0 be equal to its maximum value 1–2v during the integration (see the second term of right hand side in Eq. (22a)), the upper bound of the relative error of the integration term on the right hand side in Eq. (22a) can be obtained as

$$|\delta^U| = 1 - \frac{1}{\sqrt{1+\frac{1}{3}(1-2v)^2}^{(1-N)}\,[1+(1-2v)]^N}. \tag{23a}$$

For $N = 0.2$ and letting v be equal to 0.5, 0.4, 0.3, 0.2, 0.1, respectively, one can obtain the values of $|\delta^U|$ to be equal to 0.000, 0.041, 0.084, 0.130, 0.177, respectively.

Using M_0 and κ_e (see Eq. (19)) to normalize the moment and curvature, respectively, and considering the relationship

$$\kappa\xi = \kappa_e t/2 = \varepsilon_Y^e \tag{24}$$

from Eq. (23) we obtain

$$\frac{M}{M_0} = \left\{\frac{2}{3} - \frac{2}{N+2}\gamma\right\}\frac{1}{(\kappa/\kappa_e)^2} + \frac{2}{N+2}\gamma\left(\frac{\kappa}{\kappa_e}\right)^N, \tag{25}$$

where

$$\gamma = 2\sqrt{\frac{1}{3}(1-v+v^2)}^{1-N}(1-v)^N. \tag{26}$$

For incompressible materials, $v = 0.5$ and thus $\gamma = 1$. The expression Eq. (25) is then expected to the one proposed by Kim and Aravas (1988).

3.3. Unloading bending

Similarly, one can derive the moment–curvature relationship for unloading as

$$\frac{M}{M_0} = \frac{2}{3}\frac{\kappa - \kappa_0}{\kappa_e}, \tag{27}$$

where κ_0 is the residual curvature after the first unloading, see Fig. 1.

It is worth pointing out that generally speaking, the turning point between loading and unloading (Point B in Fig. 1) is not located at the crack tip, it locates somewhere behind the crack tip (point B for bending model). Since this point is near the crack tip of the order $O(\delta_c)$, one can consider the point B on the crack tip point in order to simplify the analysis.

Kim and Aravas (1988) discussed the moment–curvature relations for reverse bending and the second unloading step. Since the equations were too complicated, they only studied the elastic–perfectly plastic case. Here the approach proposed by Wei and Hutchinson (1998) is used. A parameter w_0 is introduced in order to characterize the effect from reverse bending. The definition of w_0 is given in the graph accompanying Fig. 1.

3.4. The curvature of detached thin film portion

From the equilibrium equation ($\kappa\,\mathrm{d}M = -P\sin(\Phi-\theta)\,\mathrm{d}\theta$) and the moment–curvature relationship, one can derive the curvature-slope angle relationship and the thin film deformation by integration. Here the curvature-slope angle relationship of the detached film unloading only needs to be derived, which will be used later for calculating the energy dissipation. Substituting Eq. (27) into the equilibrium equation and considering the definition of w_0, one can derive a relationship for the curvature-slope angle by a lengthy derivation

$$\kappa = \sqrt{[1-\cos(\Phi-\theta)]\frac{2P}{B} + (1-w_0)\kappa_0^2}, \quad \theta_B \approx \theta_{tip} \leqslant \theta \leqslant \theta_c, \tag{28}$$

where B is the bending modulus.

3.5. Summarizing the fundamental relations

At the unloading point (point B): $M = M_B, \kappa = \kappa_B$, using Eqs. (25) and (27), one have

$$\begin{cases} M_B/M_0 = \frac{2}{3}(\kappa_B - \kappa_0)/\kappa_e, \\ \kappa_0 = \kappa_B + \left(\frac{3}{N+2}\gamma - 1\right)\frac{\kappa_e^3}{\kappa_B^2} - \frac{3}{N+2}\gamma\frac{\kappa_B^N}{\kappa_e^{N-1}}. \end{cases} \tag{29}$$

From Eq. (28), the curvature at the unloading point (point B) is given by

$$\kappa_B = \sqrt{[1-\cos(\Phi-\theta_{tip})]\frac{2P}{B} + (1-w_0)\kappa_0^2}, \tag{30}$$

where the bending stiffness B is equal to

$$B = \frac{Et^3}{12(1-\nu^2)}. \tag{31}$$

The parameter $w_0 (0 \leqslant w_0 \leqslant 1)$ in Eq. (30) defined in Fig. 1 characterizes the reverse plastic behavior (or Bauschinger effect); θ_{tip} is the crack tip slope angle of the thin film.

Fundamental bending equations:

$$\text{Elastic case}: \ \frac{M}{M_0} = \frac{2\kappa}{3\kappa_e}; \tag{32}$$

$$\text{Elastic–plastic case}: \ \frac{M}{M_0} = \left\{\frac{2}{3} - \frac{2}{N+2}\gamma\right\}\frac{1}{(\kappa/\kappa_e)^2} + \frac{2}{N+2}\gamma\left(\frac{\kappa}{\kappa_e}\right)^N; \tag{33}$$

$$\text{Unloading case}: \ \frac{M}{M_0} = \frac{2}{3}\frac{\kappa - \kappa_0}{\kappa_e}. \tag{34}$$

Suppose that the substrate is rigid or that the Young's modulus of the substrate is much larger than that of thin film, using formulas from Eq. (32)–(34) and the $(M$–$\kappa)$ relationship of Fig. 1, one can obtain the plastic dissipation through calculating the area within the circuit OABCDEO in M–κ curves:

$$\begin{aligned}\Gamma^{\text{p}} = {} & \frac{1}{2}M_e\kappa_e - \frac{1}{2}M_B(\kappa_B - \kappa_0) + \left(\frac{2}{3} - \frac{2}{N+2}\gamma\right)M_0\left(\kappa_e - \frac{\kappa_e^2}{\kappa_B}\right) \\ & + \frac{2\gamma}{(N+1)(N+2)}M_0\left(\frac{\kappa_B^{N+1}}{\kappa_e^N} - \kappa_e\right) + \frac{1}{2}B\kappa_0^2 w_0.\end{aligned} \tag{35}$$

4. Bending model solutions for thin film nonlinear peeling

4.1. The double-parameter criterion $(\Gamma_0, \hat{\sigma})$

Considering that the interfacial fracture process is characterized by the cohesive zone model during the thin film peeling, as usual for elastic–plastic fracture analysis, the governing parameters of the model are often selected as $(\Gamma_0, \hat{\sigma})$ (Tvergaard and Hutchinson, 1993; Wei and Hutchinson, 1997; Wei, 2002; Wei et al., 2002). Previous researches for the elastic–plastic fracture problems have shown that the predicted results are insensitive to the selection of the cohesive zone shape parameters λ_1 and λ_2 (defined in Fig. 2(b)), therefore, in the present research we simply take them to be $(\lambda_1, \lambda_2) = (0, 1)$. One example taking different values of (λ_1, λ_2) for checking the insensitivity of the cohesive zone shape parameters will be presented later. The critical crack tip opening displacement $\delta_c = \sqrt{\delta_n^2 + \delta_t^2}$ is related to two governing parameters by the relation

$$\Gamma_0 = \hat{\sigma}\delta_c. \tag{36}$$

Thus, the moment in the thin film along the cohesive zone can be expressed as

$$M = M_B + P\sin\Phi(L-s) - \frac{1}{2}\hat{\sigma}(L-s)^2, \tag{37}$$

where L is the cohesive zone size, s is the coordinate along the zone from left to right. At crack tip $s = L$. L can be calculated during the integration procedure. Within the cohesive zone, based on the bending model the curvature can be expressed to be

$$\kappa = \frac{\mathrm{d}\theta}{\mathrm{d}s} \approx \frac{\mathrm{d}^2 w_z}{\mathrm{d}s^2}, \tag{38}$$

where w_z is the vertical displacement. Deformation conditions within the cohesive zone can be presented as

$$\begin{aligned} &w_z = 0, \quad \theta = 0, \quad \kappa = 0; \quad \text{for } s = 0; \\ &w_z = \delta_c, \quad \theta = \theta_{tip}; \quad \text{for } s = L. \end{aligned} \tag{39}$$

The solution form can be written as a function of the independent parameters through dimensional analysis as

$$\begin{cases} \frac{P(1-\cos\Phi)}{\Gamma_0} = f_1(E/\sigma_Y, \hat{\sigma}/\sigma_Y, N, v, t/R_0, w_0, \Phi), \\ \frac{Et\kappa_0}{\sigma_Y(1-v^2)} = g_1(E/\sigma_Y, \hat{\sigma}/\sigma_Y, N, v, t/R_0, w_0, \Phi), \\ \theta_{tip} = r_1(E/\sigma_Y, \hat{\sigma}/\sigma_Y, N, v, t/R_0, w_0, \Phi), \end{cases} \tag{40}$$

where a length parameter R_0 is introduced and defined as

$$R_0 = \frac{1}{3\pi(1-v^2)} \frac{E\Gamma_0}{\sigma_Y^2}, \tag{41}$$

which characterizes the plastic zone size at crack tip in the small scale yielding regime (Tvergaard and Hutchinson, 1993; Wei and Hutchinson, 1997). θ_{tip} is crack tip slope angle. If δ_c is adopted as a normalizing quantity for length in Eq. (40), from Eqs. (36) and (41) there exists a relationship between δ_c and R_0,

$$R_0 = \frac{(\hat{\sigma}/\sigma_Y)(E/\sigma_Y)}{3\pi(1-v^2)} \delta_c. \tag{42}$$

Using the relations from Eqs. (29)–(39), one can generate the detailed expressions of the solution Eq. (40) through solving the equations using an iterating process.

4.2. The double-parameter criterion (Γ_0, θ_{tip}^c)

In this case, the solution can be directly obtained from Eqs. (2), (29), (30) and (35), and by dimensional analysis. The solution form can be expressed as

$$\begin{cases} \frac{P(1-\cos\Phi)}{\Gamma_0} = f_2(N, v, t/R_0, w_0, \Phi, \theta_{tip}^c), \\ \frac{Et\kappa_0}{\sigma_Y(1-v^2)} = g_2(N, v, t/R_0, w_0, \Phi, \theta_{tip}^c), \end{cases} \tag{43}$$

which is independent of the material yield strength and Young's modulus, although the effects of them are reflected in the expression of R_0.

4.3. The double-parameter criterion ($\Gamma_0, \bar{\varepsilon}_c$)

For this case, the solution can be directly obtained from Eqs. (2), (4), (13), (15), (16), (29), (30) and (35), and by dimensional analysis, the solution form can be expressed as follows

$$\begin{cases} \frac{P(1-\cos\Phi)}{\Gamma_0} = f_3(N, v, t/R_0, w_0, \Phi, \bar{\varepsilon}_c/\varepsilon_Y), \\ \frac{Et\kappa_0}{\sigma_Y(1-v^2)} = g_3(N, v, t/R_0, w_0, \Phi, \bar{\varepsilon}_c/\varepsilon_Y), \\ \theta_{tip} = r_3(N, v, t/R_0, w_0, \Phi, \bar{\varepsilon}_c/\varepsilon_Y), \end{cases} \tag{44}$$

where $\varepsilon_Y = \sigma_Y/E$ is the yield strain.

4.4. Solutions and discussions

The solutions based on the double-parameter criterion $(\Gamma_0, \hat{\sigma})$ (cohesive zone characterization) are plotted in Fig. 4(a)–(e). Fig. 4(a)–(c) show the curves of the normalized energy release rate (or normalized

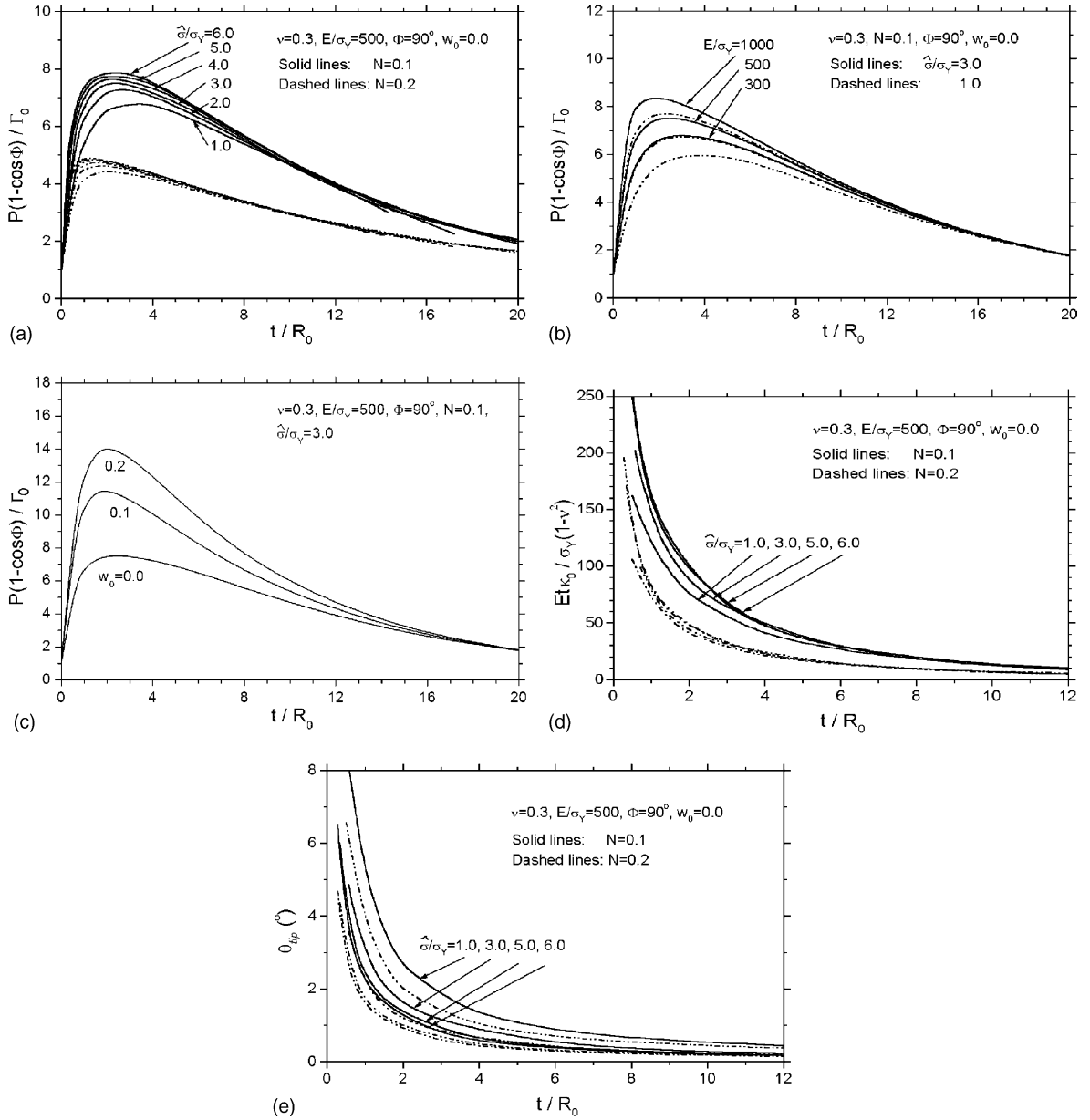

Fig. 4. Solutions of thin film peeling process based on the bending model and the criterion $(\Gamma_0, \hat{\sigma})$. (a) Variations of the normalized peel force vs. thin film thickness for several separation strengths. (b) Normalized peel force vs. thin film thickness for several yield strains. (c) Normalized peel force vs. thin film thickness for several w_0 values. (d) Curves of the normalized residual curvature vs. thin film thickness for several separation strengths. (e) Relations of thin film crack tip slope angle vs. thin film thickness for several separation strengths.

peel force) vs. the normalized thin film thickness under elastic–plastic and steady-state delamination. When thin film deforms elastically, one has $P(1-\cos\Phi)/\Gamma_0 = 1$, see Eq. (1). When thin film deforms plastically, evidently, the energy release rate (peel force) is remarkably enlarged by the plastic dissipation, and it, $P(1-\cos\Phi)/\Gamma_0$, is always larger than unity. It tends to unity when the film is either very thin or very thick. This implies that the effect of plastic dissipation can be neglected when the ratio t/R_0 is very small or very large. Starting at $t/R_0 \approx 0$, as film thickness increases, the energy release rate increases sharply and reaches a maximum value around $t/R_0 = 2$. The plastic dissipation decreases then gradually as thin film thickness increases further after $t/R_0 = 2$, and the energy release rate (or peeling force) gradually tends to unity. From Fig. 4(a), the variation of the energy release rate is sensitive to the material strain hardening index N, and surprisingly it is relatively insensitive to the interfacial separation strength, $\hat{\sigma}/\sigma_Y$, unlike conventional fracture analyses (Tvergaard and Hutchinson, 1993; Wei and Hutchinson, 1997). Fig. 4(b) shows the variation of the normalized peel force (normalized energy release rate) as a function of t/R_0 for several values of E/σ_Y. The effect of E/σ_Y on the relationship between $P(1-\cos\Phi)/\Gamma_0$ and t/R_0 is important. From Fig. 4(c), the effect of w_0 (inversely plastic bending) on the peel force is remarkable using the bending model, especially around $t/R_0 = 2$. This conclusion differs from that based on the finite element simulation model which will be shown in next section. Fig. 4(d) shows the variation of the normalized residual curvature $Et\kappa_0/\sigma_Y(1-\nu^2)$ as a function of t/R_0 for several separation strengths. As the film thickness decreases, the residual curvature increases rapidly. This implies that within this parameter range thin film undergoes considerable dissipation due to plastic bending, as discussed by Wei and Hutchinson (2003). The variation of the crack tip slope angle with normalized thin film thickness is plotted in Fig. 4(e). From Fig. 4(e), for $t/R_0 < 3$, decrease of the film thickness is accompanied by a significant increase of the slope angle at the crack tip. The slope angle decreases with increasing film thickness.

In using the bending model, the effect of cohesive zone shape parameters (λ_1, λ_2) on the relationship between $P(1-\cos\Phi)/\Gamma_0$ and t/R_0 is discussed here. The results for three different selections of (λ_1, λ_2) are plotted in Fig. 5. From Fig. 5, the normalized peel force (normalized energy release rate) relationship with t/R_0 is insensitive to the values of (λ_1, λ_2). This conclusion is consistent with that based on the researches for conventional elastic–plastic fracture problems (Tvergaard and Hutchinson, 1993; Wei and Hutchinson, 1997).

The solutions based on the double-parameter criterion $(\Gamma_0, \theta^c_{tip})$ are shown in Fig. 6(a) and (b). From Fig. 6(a), the variation of $P(1-\cos\Phi)/\Gamma_0$ as a function of t/R_0 is different from that shown in Fig. 4(a) based on the double-parameter criterion $(\Gamma_0, \hat{\sigma})$. The value of $P(1-\cos\Phi)/\Gamma_0$ increases monotonically as film thickness decreases. This result is consistent with that given by Kim and his collaborators for

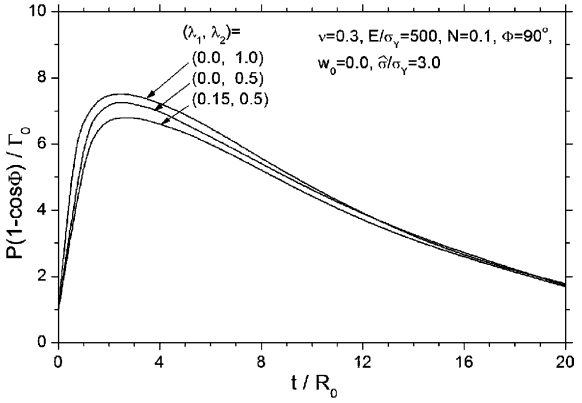

Fig. 5. Normalized peel force vs. thin film thickness for several selections of cohesive zone shape parameters.

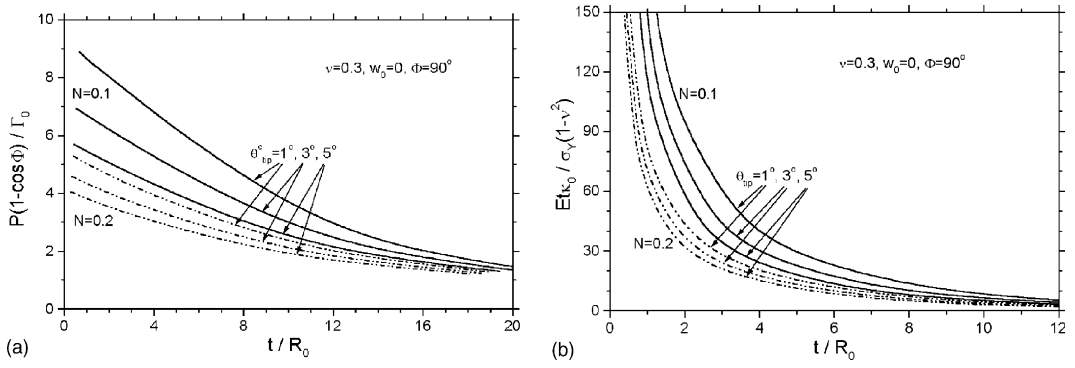

Fig. 6. The solutions of thin film peeling process based on the bending model and the criterion $(\Gamma_0, \theta^c_{tip})$. (a) Variation of normalized energy release rate vs. thin film thickness for several crack tip slope angles. (b) Relations of the normalized residual curvature vs. thin film thickness for several crack tip slope angles.

incompressible material (Kim and Aravas, 1988; Kim and Kim, 1988; Kim et al., 1989). From Fig. 6(a), the normalized energy release rate decreases as the critical slope angle increases, implying that the plastic dissipation decreases. Fig. 6(b) shows the relationship between $Et\kappa_0/\sigma_Y(1-\nu^2)$ and t/R_0. The residual curvature increases as film thickness decreases, especially for $t/R_0 < 3$, the residual curvature increases

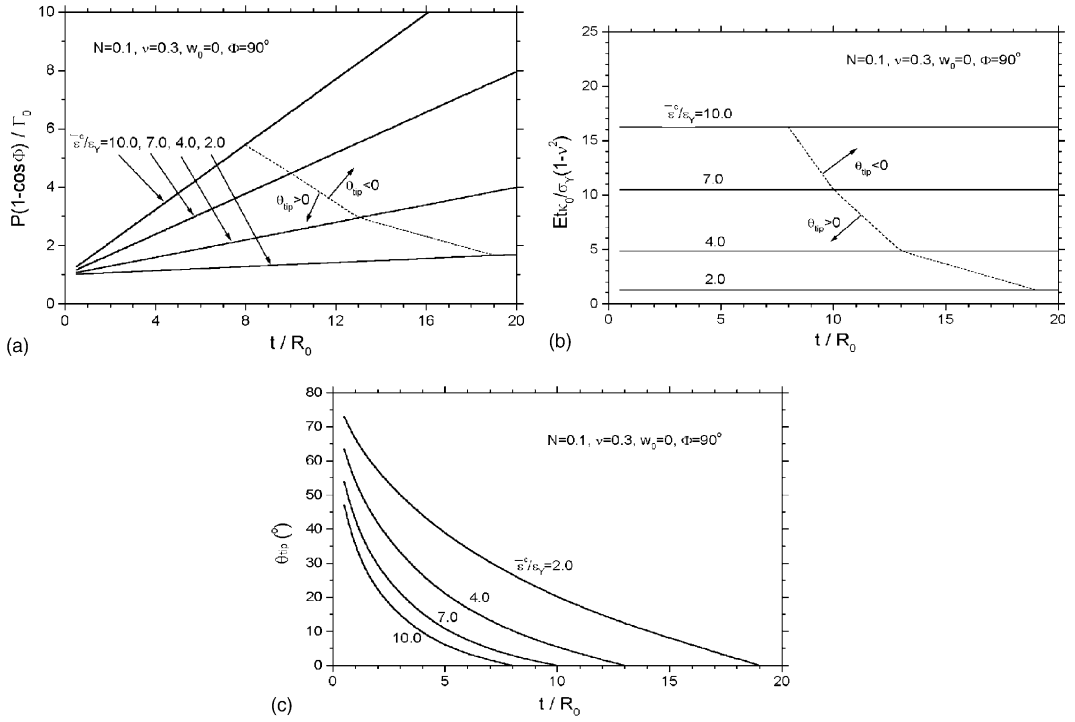

Fig. 7. The solutions of thin film peeling process based on the bending model and the criterion $(\Gamma_0, \bar{\varepsilon}_c)$. (a) Variation of the normalized energy release rate vs. thin film thickness for several critical effective strains. (b) Relations of the normalized residual curvature vs. thin film thickness for several critical effective strains. (c) Variation of the thin film slope angle at tip vs. thin film thickness for several critical effective strains.

sharply when the film thickness decreases. Obviously, there is a large plastic bending dissipation when the film thickness is small.

The results based on the double-parametric criterion $(\Gamma_0, \bar{\varepsilon}_c)$ are given in Fig. 7(a)–(c). The variation of $P(1-\cos\Phi)/\Gamma_0$ as a function of t/R_0 is much different from those shown above based on the other double-parameter criteria. In Fig. 7(a), $P(1-\cos\Phi)/\Gamma_0$ increases linearly with increasing t/R_0. The slopes of the straight lines increase with increasing $\bar{\varepsilon}_c$. Fig. 7(b) shows the variation of the normalized residual curvature with t/R_0 for several critical effective strain values. From Fig. 7(b), the normalized residual curvature is independent of the film thickness, and increases with increasing the critical effective strain. Fig. 7(c) shows the variation of the crack tip slope angle as a function of t/R_0. When the film thickness is small, the slope angle is large. With increasing film thickness, the slope angle decreases sharply and over transits to negative value. The transition points (slope angle is equal to zero) depend on the critical effective strain. Obviously, the negative slope angle of detached thin film at the crack tip is physically unaccepted. It implies that the adopted criterion is wrong when this phenomenon takes place. The reason for this problem can be interpreted as follows. Referring to Fig. 7(b), when the film thickness is small, large critical crack tip effective strain is arrived by the large bending deformation (curvature). However when film thickness is large, it is difficult or even impossible for the film to attain such large bending curvature to meet the high critical effective strain requirement.

5. Finite element analysis results for thin film nonlinear peeling

Usually for elastic–plastic fracture analysis, the fracture process zone is characterized by a cohesive zone model and the governing parameters are often taken to be $(\Gamma_0, \hat{\sigma})$ (Tvergaard and Hutchinson, 1993; Wei and Hutchinson, 1997; Wei, 2002; Wei et al., 2002). Similarly, for the present thin film peeling process, the cohesive zone model is adopted, and the governing parameters are still selected as $(\Gamma_0, \hat{\sigma})$. For this problem, elastic–plastic and two-dimensional finite element analysis model has been adopted by Wei and Hutchinson (1998). This method can be delineated briefly here. Referring to Fig. 1, the detached portion on the right side of cross-section 1 is treated with the bending model, while the other portions including thin film on the left of cross-section 1 and substrate are treated with the finite element simulation. The bending model solution for the detached portion on the right side of cross-section 1 is applied on the cross-section 1 when the second problem is simulated by using the finite element method. The total solution form with independent parameters is given by Eq. (40) (or see Wei and Hutchinson, 1998). The corresponding results for the normalized peel force (normalized energy release rate), residual curvature as well as the crack tip slope angle have already been presented by Wei and Hutchinson (1998), and these results are shown again in Fig. 8(a)–(d). For comparison with the bending model solutions, Fig. 8(a) shows the variation of $P(1-\cos\Phi)/\Gamma_0$ as a function of t/R_0 for three values of N. The results are significantly different from the bending model results given in last section. From Fig. 8(a), the normalized peel force increases with increasing the film thickness for $t/R_0 < 6$. For $t/R_0 > 6$, the normalized peel force becomes independent of the film thickness, and tends to the small scale yielding solution. Fig. 8(b) shows the variation of $P(1-\cos\Phi)/\Gamma_0$ as a function of t/R_0 for different values of w_0 (inversely plastic bending effect). From Fig. 8(b), there is a certain effect from w_0 on the normalized peel force, however the variation trends of relationship between $P(1-\cos\Phi)/\Gamma_0$ and t/R_0 for different values of w_0 are similar. Comparing the results shown in Fig. 8(b) and 4(c), the inversely plastic bending effect based on the finite element analysis model is much smaller than that based on the bending model. Fig. 8(c) shows the variation of the normalized residual curvature with t/R_0. From Fig. 8(c), the residual curvature decreases with increasing the film thickness slowly and not sharply, unlike the bending model solution. Fig. 8(d) shows the variation of the crack tip slope angle with t/R_0. The slope angle decreases slowly with increasing film thickness. From Fig. 8(c) and (d), the effects of w_0 on the residual curvature and the crack tip slope angle

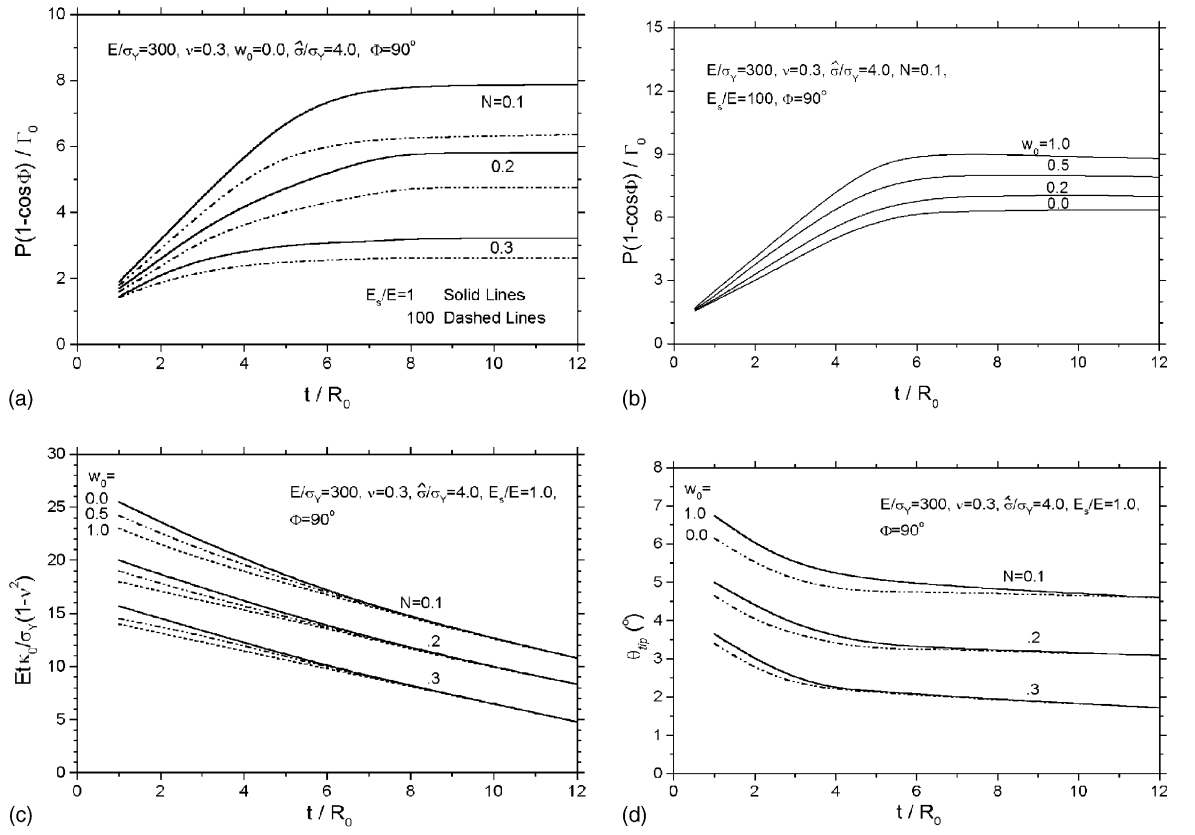

Fig. 8. The variations of the normalized peel force (a, b), residual curvature (c) and the crack tip slope angle (d) vs. the thin film thickness based on the two-dimensional finite element analysis model, from Wei and Hutchinson (1998).

are very weak based on the finite element analysis model. Comparing Fig. 8(c) with Figs. 4(d) and 6(b), clearly, the calculated residual curvature based on the finite element method is much smaller than that based on the bending model. This implies that the contribution of the plastic bending dissipation to the energy release rate based on the finite element analysis model is much smaller than that based on the bending model.

In order to further investigate and compare the solution features of thin film peeling process based on the bending model and based on the finite element analysis model, the finite element analysis model is adopted here for studying the effects of E/σ_Y (yield strain $\varepsilon_Y = \sigma_Y/E$) on the relationship between $P(1-\cos\Phi)/\Gamma_0$ and t/R_0, and for studying very large ratio t/R_0. The results are plotted in Figs. 9 and 10 for a strong separation strength ($\hat{\sigma}/\sigma_Y = 4$) and for a weak separation strength ($\hat{\sigma}/\sigma_Y = 1$), respectively. The difference between results shown in Fig. 9(a) and (b) only lies in the range of t/R_0 plotted in the curves. Obviously, the peel force (energy release rate) is very sensitive to the value of E/σ_Y. From Fig. 9(b), when film thickness is very large, i.e., for $t/R_0 > 15$, the peel force slowly decreases with increasing t/R_0. Fig. 10 shows the simulation results for a weak interface ($\hat{\sigma}/\sigma_Y = 1$). The difference between results shown in Fig. 10(a) and (b) is only in the range of t/R_0. From Fig. 10(a), for $t/R_0 < 12$, the normalized peel force increases as t/R_0 increases first, then tends to constant as t/R_0 increases further, independent of t/R_0 within a certain region. However, for $t/R_0 > 15$, increasing t/R_0 further decreases the normalized peel force to tend to unity for very large film thickness.

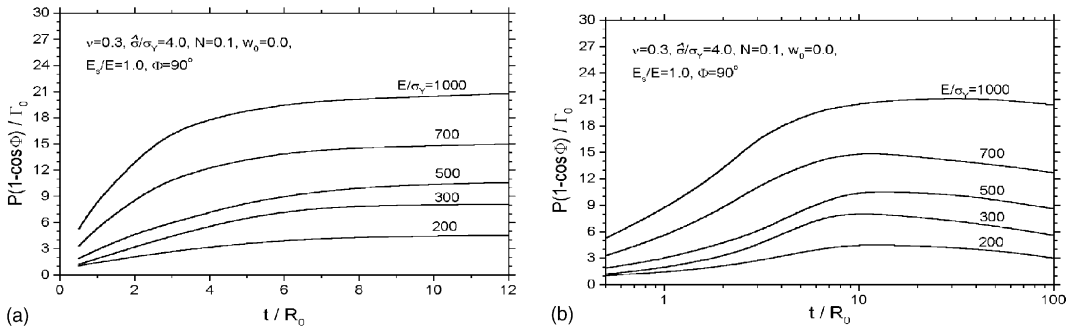

Fig. 9. Relations of the normalized energy release rate vs. the thin film thickness for several material yielding strain values ($\varepsilon_Y = \sigma_Y/E$) and for a strong interfacial adhesion case. The results based on the two-dimensional finite element analysis model for conventional film thickness region (a) and for a large film thickness region (b).

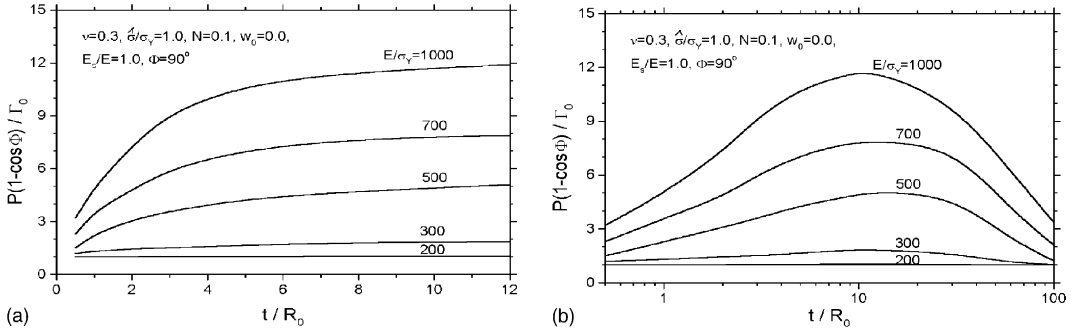

Fig. 10. Variations of the normalized energy release rate vs. the thin film thickness for several material yielding strain values ($\varepsilon_Y = \sigma_Y/E$) and for a weak interfacial adhesion case. The results based on the two-dimensional finite element analysis model for conventional film thickness region (a) and for a large film thickness region (b).

6. Discussions and conclusions about modeling thin film nonlinear peeling

Solutions for thin film nonlinear peeling process have been revealed in Sections 4 and 5 based on both the bending model with three different double-parameter criteria, and the elastic–plastic finite element analysis model with the cohesive double-parameter criterion. There exists very big difference between the bending model solutions for three double-parameter criteria. Obviously, the bending model solutions are very sensitive to the selection of the governing parameters. This leads to a serious question: what is a reasonable selection of the governing parameters for predicting the thin film nonlinear peeling in using a bending model? From the solutions based on the first two double-parameter criteria as shown in Figs. 4–6, when normalized film thickness is smaller than about 5, $t/R_0 < 5$, the contribution of plastic bending dissipation to the energy release rate is very large. This can be confirmed from the obtained high values of the residual curvature, Figs. 4(d) and 6(b). The residual curvatures shown in these figures are much larger than those shown in Fig. 7(b) based on the third criterion or shown in Fig. 8(b) based on the finite element analysis model. From the solutions based on the bending model and the third criterion, when normalized film thickness is smaller than about 5, $t/R_0 < 5$, the contribution of the bending plastic dissipation to energy release rate is obviously smaller than that based on the bending model and the first or second criterion. Let us compare the bending model results shown in Figs. 4–7 with the elastic–plastic finite element analysis

results shown in Figs. 8–10. The bending model results based on the third double-parameter criterion (the interfacial fracture toughness and the critical Mises effective strain) is the most accurate within the range of $t/R_0 < 5$. As film thickness increases further, i.e., for $t/R_0 > 5$, the results of the elastic–plastic finite element calculation show towards the small scale yielding solution (insensitive to the film thickness), while the bending model solution based on the third double-parameter criterion still increases linearly with t/R_0, and the criterion becomes invalid, as discussed in last section. It is interesting to compare the results shown in Figs. 4(a) and (b) and 10(b) when adhesion between thin film and substrate is weak, i.e., for $\hat{\sigma}/\sigma_Y = 1$. The normalized peel force, $P(1-\cos\Phi)/\Gamma_0$ reaches a maximum value at about $t/R_0 = 15$ based on the finite element analysis model from Fig. 10(b), however, the normalized peel force reaches the maximum value at about $t/R_0 = 2$ based on the bending model from Fig. 4(a) and (b). Comparing Fig. 9(b) with Fig. 10(b), the small scale yielding solution within a range of the film thickness ($5 < t/R_0 < 13$) tends to be preserved as adhesion strength ($\hat{\sigma}$) increases, when film thickness is very large.

The following main conclusions are established from the present analyses.

(1) The peeling test solutions based on bending model are very sensitive to the selection of the governing parameters.
(2) The prediction for peeling test problem based on the bending model and based on the double-parameter criterion $(\Gamma_0, \bar{\varepsilon}_c)$ shows the most accurate within the range of $t/R_0 < 5$ by comparing the prediction based on the elastic–plastic finite element analysis model. However, the double-parameter criterion $(\Gamma_0, \bar{\varepsilon}_c)$ becomes invalid for $t/R_0 > 5$.
(3) An effective bending model criterion for $t/R_0 > 5$ needs to be explored further.

Acknowledgements

This work was supported by the National Natural Science Foundation of China through Grant 19925211, and jointly supported by the Chinese Academy of Sciences through "Bai Ren Plan".

References

Asai, H., Iwase, N., Suga, T., 2001. Influence of ceramic surface treatment on peel-off strength between aluminum nitride and epoxy-modified polyaminobismaleimide adhesive. IEEE Trans. Adv. Pack. 24, 104–112.

Betegon, C., Hancock, J.W., 1991. Two-parameter characterization of elastic–plastic crack-tip fields. J. Appl. Mech. 113, 104–110.

Bundy, K., Schlegel, U., Rahn, B., Geret, V., Perren, S., 2000. Improved peel test method for measurement of adhesion to biomaterials. J. Mater. Sci.: Mater. Med. 11, 517–521.

Choi, J.W., Oh, T.S., 2001. Peel strength and peel angle measured by the *T*-peel test on Cr/BPDA-PDA interface. J. Adhes. Sci. Technol. 15, 139–152.

Cotterell, B., Williams, G., Hutchinson, J., Thouless, M., 2002. Announcement of a round robin on the analysis of the peel test. Int. J. Fract. 114, L9–L13.

Feliu-Baez, R., Lockhart, H.E., Burgess, G., 2001. Correlation of peel and burst tests for pouches. Pack. Technol. Sci. 14, 63–69.

Kawabe, M., Tasaka, S., Inagaki, N., 2000. Effects of surface modification by oxygen plasma on peel adhesion of pressure-sensitive adhesive tapes. J. Appl. Polym. Sci. 78, 1392–1401.

Kim, K.S., Aravas, N., 1988. Elasto-plastic analysis of the peel test. Int. J. Solids Struct. 24, 417–435.

Kim, K.S., Kim, J., 1988. Elasto-plastic analysis of the peel test for thin film adhesion. J. Eng. Mater. Technol. 110, 266–273.

Kim, J., Kim, K.S., Kim, Y.H., 1989. Mechanical effects of peel adhesion test. J. Adhes. Sci. Technol. 3, 175–187.

Kinloch, A.J., Lau, C.C., Williams, J.G., 1994. The peeling of flexible laminates. Int. J. Fract. 66, 45–70.

Moidu, A.K., Sinclair, A.N., Spelt, J.K., 1998. On determination of fracture energy using the peel test. J. Test. Eval. 26, 247–254.

O'Dowd, N.P., Shih, C.F., 1991. Family of crack tip fields characterized by a triaxiality parameter—I. Structure of fields. J. Mech. Phys. Solids 39, 989–1015.

Park, I.S., Yu, J., 1998. An X-ray study on the mechanical effects of the peel test in a Cu/Cr/polyimide system. Acta Mater. 46, 2947–2953.

Rice, J.R., 1974. Limitations to the small scale yielding approximation for crack tip plasticity. J. Mech. Phys. Solids 22, 17–26.

Spies, G.J., 1953. The peeling test on redux-bonded joints. J. Aircraft Eng. 25, 64–70.

Tvergaard, V., Hutchinson, J.W., 1993. The influence of plasticity on mixed mode interface toughness. J. Mech. Phys. Solids 41, 1119–1135.

Wei, Y., 2002. Thin layer splitting along the elastic–plastic solid surface. Int. J. Fract. 113, 233–252.

Wei, Y., Hutchinson, J.W., 1997. Nonlinear delamination mechanics for thin films. J. Mech. Phys. Solids 45, 1137–1159.

Wei, Y., Hutchinson, J.W., 1998. Interface strength, work of adhesion and plasticity in the peel test. Int. J. Fract. 93, 315–333.

Wei, Y., Hutchinson, J.W., 2003. Peel test and interfacial toughness. In: Gerberich, W.W., Yang, W. (Eds.), Encyclopedia of Comprehensive Structural Integrity, vol. 8. Elsevier Science, Oxford, pp. 181–217 (Chapter 5).

Wei, Y., Wang, T.C., 1995. Fracture criterion based on the higher-order asymptotic fields. Int. J. Fract. 73, 39–50.

Wei, Y., Zhao, M., Tang, S., 2002. Characterization of the fracture work for ductile film undergoing the micro-scrach. Acta Mech. Sinica 18, 494–505.

Yang, Q.D., Thouless, M.D., Word, S.M., 1999. Numerical simulations of adhesively-bonded beams failing with extensive plastic deformation. J. Mech. Phys. Solids 47, 1337–1353.